On the experimental generation of focusing wave groups on following and adverse sheared currents in a wave-current flume

Dimitris Stagonas(1), Eugeny Buldakov(2), Richard Simons(3)

(1) Research Associate, Department of Civil, Environmental and Geomatic Eng., University College London, UK, d.stagonas@ucl.ac.uk

(2) Lecturer, Department of Civil, Environmental and Geomatic Eng., University College London, UK, e.buldakov@ucl.ac.uk

(3) Professor, Department of Civil, Environmental and Geomatic Eng., University College London, UK, r.r.simons@ucl.ac.uk

Abstract

Focused waves are often used in physical and numerical studies as a representative condition for extreme waves or as a means to generate very steep and breaking waves at a prescribed location in space and time. They have also been combined with depth-varying currents in investigations of incipient wave breaking, wave breaking induced energy dissipation, and wave-current induced loads on marine structures. A focused wave is created when all the components in a transient wave group come into phase. In the past, linear wave theory and iterative methodologies coupled with the linear Doppler-shifted dispersion relationship have been suggested to account for the presence of a current and achieve the required phase and amplitude focusing. In the majority of cases linear or constant steepness spectra are used, which compared to the measured or theoretical spectra like JONSWAP (Joint North Sea Wave Project), Gaussian and Pierson-Moskowitz (PM) can be termed as unrealistic. The effectiveness of these methodologies also decreases as the nonlinearity increases and therefore in most studies either weakly nonlinear conditions are employed or the focus location is determined empirically. Here, an iterative methodology is suggested which can focus waves of any height at a predetermined temporal and spatial location even for wave groups propagating on a strong following or adverse current. An experimental apparatus developed to generate relatively stable sheared velocity profiles is also described. The depth varying profile of the resulting currents diverges from that of classical wind driven currents and comes closer to profiles measured in field sites important for the deployment of, for instance, tidal and wind energy converters. The methodology is successfully applied to wave groups travelling on still water, following and adverse currents, and the results presented refer to linear, weakly nonlinear and strongly nonlinear focused waves generated for a range of realistic target spectra. The capability to generate wave groups with the same amplitude spectrum

at a fixed location for a variety of flow conditions - still water, following and adverse sheared currents – is also illustrated.

Introduction

The constructive interference at a certain point in space and time of numerous wave components of varying frequency and amplitude results in the generation of a large focused wave. When simulating extreme hydrodynamic conditions in a laboratory facility, such a wave possesses comparative advantages. It is significantly higher and steeper than any other wave within the propagating wave group, it occurs at a predefined point in space and time, and it represents an event with a large return period which may take a long time to reproduce within a random wave sequence. Hence the deterministic nature of focused waves makes them suitable candidates for design waves in experimental and analytical investigations of wave loading on marine structures (Tromans et al., 1991).

Oceanic field measurements (Taylor and Williams, 2002; Christou and Ewans, 2014) have confirmed previous theoretical considerations (Lindgren, 1970) linking the occurrence of the largest waves to propagating waves groups. On many occasions wave groups will co-exist with currents. In fact, the interaction of wave groups with currents is among the physical mechanisms proposed to explain the formation of rogue waves (Bretherton and Garrett, 1968; Peregrine 1976). For relatively shallow water and relatively strong tidal flows there will be a considerable difference to the flow resistance from the seabed upwards, leading to a sheared current. The presence of surface shear has been associated with variations in the steepness and shape of wave crests, and incipient breaking (Banner and Song, 2002). The combination of very steep and potentially overturning waves with sheared currents entails the local formation of very fast flow regions and thus the potential exposure of marine structures to unusually high forces.

Despite its importance, however, experimental investigations on the interaction of waves and especially focused wave groups with sheared currents are scarce. Challenges associated with the generation under laboratory conditions of sheared currents, strongly nonlinear focused waves, and both combined seem to be the main reason for this shortage in measurements. The simultaneous generation of waves and depth-varying currents requires the minimum of interaction between the flow-shaping apparatus and the generated/propagating waves. Usually PVC plates, layers of polyether foam, and honeycomb blocks are used to condition and straighten the current. The required depth-varying velocity profile is provided through the combination of solid and perforated PVC plates of varying heights extending from the bed up to about 10cm below the free surface (Swan et al., 2001; Yao and Wu, 2005). Therefore, the selection of testing conditions is restricted to waves for which the underlying wave kinematics are not drastically disturbed by the flow conditioner/straightener. Wave reflection is an additional problem, mainly for waves generated on adverse currents.

For the focusing of experimental unidirectional wave groups three main approaches can be identified. For the simplest approach, linear wave theory is used to calculate the phases of the wave components at the inlet required to produce a wave group focusing at a preselected time and location in the flume (Rapp and Melville, 1990). Empirical methods have also been proposed, where the numerical input for the wavemaker is corrected through an iterative process using surface elevation measurements at the focal point. The Fourier transformation of the elevation time history is used together with the target spectrum to calculate the corrected phases for the new input and the scheme is repeated until all wave components come into phase at focus (Chaplin, 1996). The latter approach was extended to include amplitude modification, and more recently a self-correcting method employing a potential flow solver to replace the physical re-production of the wave groups required for the iterations was suggested (Schmittner et al., 2009; Fernandez et al., 2014). In a different method, the wave board signal required for the generation of a focused wave was computed by backward integration of the Zakharov equation (Shemer et al., 2007). For focusing wave groups in the presence of currents, the empirical method of Chaplin (1996) has been modified to include a linear dispersion relation accounting for the presence of a current with a constant shear (Yao and Wu, 2005).

Although effective for small amplitude waves, the efficiency of these methods reduces as the nonlinearity of the wave group increases. As a result, for increasing focused wave amplitudes, the focal point is shifted in both space and time and the quality of focusing reduces considerably.

Experimental results with focusing wave groups show that both the location and time of the focused event are dependent upon the nonlinearity of the wave group. Compared to linear prediction, a downshift of up to 1.6m for the focal point and a time-shift of up to 0.6sec for the focusing time were reported (Baldock et al., 1996). It is also noted that, with some exceptions, previous methods have been used with unrealistic target spectra such as top-hat or constant slope; in this work spectra with the same shape as one of the measured/theoretical spectra available in the existing literature (for example JONSWAP (JS), Pierson-Moskowitz (PM) and Gaussian (GS)) are referred to as realistic. The present work combines and adds to previous knowledge and proposes a new methodology and experimental apparatus which increase control over the generation of unidirectional focusing wave groups on following and adverse sheared currents in a wave-current flume. Previously, this approach has been used successfully to generate focused waves on still water and on a following current using a Gaussian target spectrum with peak frequency of 0.6Hz (Stagonas et al., 2014). In the current article, the methodology and the experimental apparatus are described in detail: the cases considered increase substantially to include adverse currents, four different targets including spectra with high frequency tails, and two different peak frequencies per spectrum resulting in wave components travelling on shallow, intermediate and deep water conditions. The proposed methodology is described first before presenting the flow-shaping apparatus that allows the creation of sheared currents with a significantly reduced effect on wave generation. This is followed by an example application and results.

Wave focusing methodology

For wave generation in flumes using a desired target spectrum, linear or 2nd order wave theory is usually combined with the appropriate transfer functions to calculate the required displacement of the wavemaker. However, for strongly nonlinear waves the interaction between the wave components of a propagating wave group reshapes the amplitude spectrum in a way which is not predicted by either linear or 2nd order wave theory, e.g. (Baldock et al., 1996). Complexities increase further for wave groups on currents as, in addition to wave-wave interactions, wave-current interactions also occur and affect the evolution of both the amplitude and phase spectrum (Dingemans, 1997). Empirical methodologies use surface elevation measurements to produce a corrected input signal for the wavemaker and through trial and error overcome the limited capacity of existing wave-current theories to accurately predict the spectral evolution of wave groups on sheared currents (Chaplin, 1996). Along these lines, linear wave theory has also been combined with a 2nd order wave-current dispersion equation to generate focused waves on sheared currents (Yao and Wu 2005). As with every other empirical approach, however, corrections were calculated using the fully nonlinear surface elevation signal, which resulted in limited success for strongly nonlinear conditions.

In this paper an iterative procedure is described for generating focused wave groups with a target spectrum over currents. The use of a linearised input signal instead of a fully nonlinear wave record distinguishes the proposed methodology from previous attempts. A linearized input signal is the natural choice since the full spectrum of a nonlinear wave group is uniquely defined by its linear part, and since it can be accurately reproduced by any wavemaker employing linear wave theory.

Additional key features of the methodology include the use of realistic target spectra and the possibility of using different wave probes for phase and amplitude iterations. For example, for wave groups generated over still water, following and adverse currents, the linearized amplitude spectra can be corrected to match the target spectrum at a point near the wavemaker, while the phase spectra are corrected to zero at a location far away from the wavemaker; hereafter, we refer to the former location as the Amplitude Matching Point (AMP) and to the latter as the Focusing Point (FP).

The reasons for separating AMP (Amplitude Matching Point) and FP (Focusing Point) are twofold. Nonlinear wave-wave and wave-current interactions modify the wave group as it travels along the flume. These modifications are usually manifested as energy transfers from lower to higher frequencies and thus attempting to match an amplitude spectrum to the target far away from the wavemaker may entail the generation of a wave group with a non-physical spectrum, especially for high frequency wave components. Therefore, control over the amplitudes and phases of these components is reduced. In addition, increased dissipation of high frequency components along the flume will result in generation of excessively steep high frequency waves leading to premature breaking.

At the same time, selecting the AMP to be near the wavemaker and the FP further away provides the opportunity to generate wave groups on variable flow conditions –still water, following/adverse currents with different characteristics - with initially the same linearized amplitude spectrum. Practical experience has shown that setting the AMP at a small distance from the inflow/outflow is beneficial, as it allows for the wave to interact with the flow and develop naturally as it propagates towards the

FP. This way, stability and convergence of iterations improves and natural features of the wave group's interaction with following and adverse currents develop.

The proposed methodology consists of 4 main steps. For the 1st iteration the target spectrum is used as the initial input to the control system. Here, spectra with and without equilibrium tails such as Gaussian, JONSWAP and PM are used as targets, but the use of arbitrary spectra is also theoretically possible. Then, the following steps apply to all subsequent iterations. Firstly for each amplitude spectrum four wave groups are generated with constant phase shifts of $\Delta\Phi = 0$ (crest focused wave), π (trough focused wave), $\pi/2$ and $3\pi/2$ (positive and negative slope focused waves). The surface elevation for each group is measured at the AMP and the FP and the phase-shifted signals are spectrally decomposed as described later in this section to obtain the linearised signal. The amplitudes and phases of the linearised spectrum are compared with the target spectrum and a corrected input spectrum is calculated from:

$$a(f_i)_{in}^{n} = a(f_i)_{in}^{n-1} \times a(f_i)_{tgt} / a(f_i)_{out}^{n-1} \qquad \text{Eq. 1}$$

$$\phi(f_i)_{in}^{n} = \phi(f_i)_{in}^{n-1} - (\phi(f_i)_{tgt} - \phi(f_i)_{out}^{n-1}) \qquad \text{Eq. 2}$$

where $a(f_i)_{in}^{n}$ and $\phi(f_i)_{in}^{n}$ are the input amplitude and phase of the i^{th} frequency of the linearised spectrum for the n^{th} iteration; $a(f_i)_{in}^{n-1}$ and $\phi(f_i)_{in}^{n-1}$ are the input amplitude and phase of the i^{th} frequency of the linearised spectrum for the n^{th}-1 iteration; $a(f_i)_{tgt}$ and $\phi(f_i)_{tgt}$ are the target amplitude and phase for the i^{th} frequency, and $a(f_i)_{out}^{n-1}$ and $\phi(f_i)_{out}^{n-1}$ are the output/measured amplitude and phase of the i^{th} frequency of the linearised spectrum for the n^{th}-1 iteration. Iterations continue until the spectral components of the linearised signal come into phase at the FP and their amplitudes at the AMP match those of the target spectrum to the desired accuracy. For the experiments with waves on sheared currents considered in the present article, measured amplitudes and phases converged to ±3% of the target within 2 to 3 iterations. As illustrated in the Application Example section below, the number of iterations required depends on the nonlinearity of the wave, while the accuracy, convergence and overall reliability of iterative focusing techniques is discussed in detail in (Buldakov et al. 2017).

Although somewhat laborious, the methodology ensures that through the iterations a ‘self-calibration’ of the wavemaker is performed for any flow condition in the flume. As an example, and for a wavemaker controlled by directly specifying the time history of its displacement, one would expect that a different calibration is required for still water, following and adverse currents. Nevertheless, through the iterative correction of the input signal a re-calibration of the wavemaker when transferring from, for example, still water to following flow conditions is no longer required. When the iterations are converged the same target output is achieved for all flow conditions at the AMP and FP, without the need to compute new transfer functions.

Spectral decomposition, also known as separation of harmonics, is a powerful technique for isolating harmonic components corresponding to Stokes expansion orders. For example, two wave profile time-histories with a constant phase shift of π corresponding to peak and trough focused wave groups can be used to separate even and odd harmonics in the measured surface elevation. In this separation, second order sub- and super-harmonics co-exist in the same record (even harmonics), and the same is true for linear, 3rd and higher order terms (odd harmonics) (Borthwick et al., 2006; Orszaghova et al., 2014). Hence, the signal decomposed in such a way is difficult to use for the calculation of the corrected input as the linearised part is contaminated by higher order nonlinear terms. More recently, combinations of more than 2 experimental records have been used confirming the possibility of a more effective separation of components either in the time or in the frequency domain (Hann et al. 2014; Fitzgerald et al. 2014).

In the present study the following 4-wave decomposition is used to separate first and higher-order wave components:

$$S_0 = \frac{s_0 + s_1 + s_2 + s_3}{4}$$
$$S_1 = \frac{s_0 - is_1 - s_2 + is_3}{4}$$
$$S_2 = \frac{s_0 - s_1 + s_2 - s_3}{4} \qquad \text{Eq. 3}$$
$$S_3 = \frac{s_0 + is_1 - s_2 - is_3}{4}$$

where s_n are complex spectra of fully nonlinear surface elevation signals with phase shifts $\pi n/2$, n=0,1,2,3; S_0 is the complex spectrum of the 2nd order difference components; and $S_{1,2,3}$ are complex spectra of nonlinear super-harmonics for 1st (linear), 2nd and 3rd orders.

An example of the 4-wave spectral decomposition application to wave groups generated with a wideband Gaussian target spectrum is illustrated in Figure 1. In particular, the time histories of surface elevation for $\Delta\Phi = 0$, π, $\pi/2$ and $3\pi/2$ at the AMP and the FP are presented in Figures 1 (a) and (c). These records are used to decompose the spectrum into its linearised (S_1) and nonlinear ($S_{0,2,3}$) parts shown in Figures 1 (b) and (d). It is noteworthy that for a 4-wave decomposition the 1st order (linearized) part includes 5th and higher order terms (see Eq. 3), which however have insignificant amplitudes.

An example of the inverse Fourier reconstructed elevation time histories of the 1st (linearized) order, 2nd order sum and difference and 3rd and higher order waves for wave groups propagating on still water (solid line), adverse (dashed line) and following current (dotted line) is illustrated in Figure 2. Spurious and reflected waves are clearly distinguished from the free and bound waves of the focused crest, and can thus be excluded by selecting an appropriate analysis/observation window for the iterations. Previously, the contamination of the measured signal with unwanted waves was a significant challenge for any empirical methodology. Here, the ability to exclude them leads to better control over the wave group and improves convergence.

The effects of wave-current interaction on the evolution of wave groups are evident in Figure 2. In Figure 2 (a), and for the time instant between ±3sec, the highest linearized focused event is seen for the group propagating on an adverse current (dashed line). Since the linearised amplitude spectra for all cases illustrated are matched at the AMP with high accuracy, the differences observed can be attributed to the effect of the current on the waves as they propagate from the AMP to the FP. The higher energy content of the linearized part agrees well with the reduced amplitudes observed for the second-order sum and third and higher order components of the same group, as shown in Figures 2 (b) and (d).

The long wave trough is also seen to be deeper/shallower for the tests on following/adverse current (dotted/dashed lines), while the amplitude and width of the long wave crest is significantly reduced/increased. Since, however, for these experiments – employing linear wave generation – second-order difference components are inevitably contaminated with spurious long wave components, it is not possible to comment on their connection to the evolution of the linearized part; it is also noted that spurious second-order sum components travel with a celerity smaller than that of the group and they are thus separated at focus, see for instance prior to -3sec in Figure 2 (b). Local nonlinear effects responsible for the formation of bound higher-order components are different for different current conditions and result in discrepancies between higher-order components close to t = 0sec. Similarly, spurious free and reflected components are also different for different current conditions explaining differences at times after and before the main event at focus for second-order difference components. Nevertheless, a detailed investigation of these aspects of wave-current interaction falls outside the scope of this paper.

Experimental apparatus for generating sheared currents in a wave-current flume

The wave-current flume at UCL is 20m long, 1.2m wide and 1m deep. It is equipped with two Edinburgh Design Limited force-feedback 'piston-type' wavemakers, installed at each end of the flume. One wavemaker is used to generate waves, while the other acts to absorb the incoming wave energy. Three impellers placed in parallel recirculation pipes are used to drive the flow, which enters and exits the tank vertically. The flow is discharged in the working section of the flume at a distance of1m in front of each wavemaker, and through a 0.4m deep settling tank fitted with turning vanes and a honeycomb, Figure 3.

At the inflow point of 'up-welling' type facilities such as the UCL wave-current flume, the free surface is significantly perturbed and leads to increasingly unsteady conditions as the flow speed increases. This in turn has an undesirable effect on wave generation and propagation. At the outflow, a vortex is formed with a size and intensity which increases with the flow speed and results in further unsteadiness of the free surface upstream. For 'up-welling' type facilities a delay in flow development due to the formation of a strong recirculation pattern at the inlet has been previously reported, (Robinson et al. 2015). The flow was shown to acquire the uniform velocity desired for their study about 40m downstream from the inlet. Turbulence intensity increased from about 12% to its maximum 20% within the first 10m, while an additional 10m (20m from inlet) were required for its values to reduce below 15%. Following (Giles et al. 2011), representative real sea conditions can be achieved in experimental facilities only if turbulence intensity in the working section is less than 10-15%. Flow development and test repeatability is also negatively affected by high turbulence levels, and the challenges increase further if sheared currents are to be produced. Nevertheless, sheared currents have more practical applications than uniform or logarithmic currents which are most commonly considered in wave-current experiments.

The Pentland Firth is a typical example where strong wave-current interaction phenomena occur and affect the deployment of tidal turbine arrays. If the typical conditions in the Pentland Firth are scaled to the size of the UCL flume, then for a water depth of 0.5m the current will have an equivalent velocity of 0.2m/s near the surface. These calculations are based on ADCP field measurements, which also confirm that the shear in these flows differs from the typical wind generated shear, with a collinear reduction of the velocity with depth (Chatzidou and Karunarathna, 2014). In contrast, profiles for wind generated sheared flows are closer to those used in previous studies, where the current speed is high very close to the free surface and reduces to zero less than half way through the water depth (Swan et al., 2001; Yao and Wu, 2005).

Wire mesh structures have been successfully used to generate controlled and reproducible regular waves over uniform currents (Kemp and Simons, 1982; Kemp and Simons, 1983). This concept is developed further in the present study to accommodate the requirement to generate sheared currents. The flow conditioning/shaping apparatus shown in Figure 4 consists of 8cm diameter tubes made of flexible galvanised wire mesh with 5cm holes. A 0.5m long, 1.2m wide and 0.88m deep box section formed of vertically and horizontally placed tubes is positioned on top of the inlet/outlet at each end of the flume. An additional filter layer is installed between the pre-existing honeycomb and the box section to further condition the flow. The filter is made of a 5cm thick, 50Pores Per Inch (PPI) polyester foam enclosed between two anodized aluminum meshes with 1cm holes. The additional flow resistance required to generate a sheared profile is introduced by a triangular 0.88m x 0.88m section made of the same wire mesh tubes and attached to the downstream side of the box section; for simplicity we refer to the triangular section as the flow profiler and the rest of the structure as the flow conditioner.

The performance and the required shape of the flow conditioner and the profiler were determined through a series of trial and error tests. A Nortek-AS Vectrino+ ADV was used to acquire flow measurements at 4m (AMP), 6.9m, 8.7m (FP) and 13m from the wavemaker, with the first and the last positions located 1m from the end of the profilers at each end of the flume. To characterize the flow, velocity profiles were measured through the vertical, starting about 2cm from the bed and extending up to about 4cm below the free surface. At each point the mean velocity was calculated from 3min long records acquired at the instrument's maximum sampling frequency of 25Hz, a measurement volume of 9.2mm and acoustic pulse length of 2.4mm; for locations with higher turbulence, such as very close to the inlet, the size of the measurement volume and the length of the acoustic pulse were reduced. Seeding was provided with rutile titanium dioxide pigment and only data with correlation values higher than 85% were considered. Mean velocity values were calculated for at least 4000 samples.

For the accurate characterization of the flow the use of higher sampling rates and records with more samples is typically recommended, see for example (Rusello et al., 2006; Chanson et al., 2007). To assess the effect of shorter records on mean velocity and maximum turbulent intensity calculations, 9min long records were also acquired for the same flow conditions. Calculations were then conducted using the full record but also 3min long segments and results were compared with those for the original data set. Differences in the mean velocity and maximum turbulent intensity were found never to exceed 0.8% and 1.5%, respectively. A similar analysis but using 30min long records was performed to ensure that the flow measurements reported are not contaminated by transient effects associated with the start and operation of the flume and/or large scale turbulent structures. Indeed, for measurements conducted at least 10min after the initiation of the flow the error in the mean velocity was less than 5%. Nonetheless, for all experiments a minimum delay time of 20min was kept between the initiation of the flow and data acquisition.

Velocity profiles at the 4 measuring locations along the flume and the 3 locations across the flume are presented in Figure 5. Sheared currents with surface velocities of ±0.2m/s and ±0.4m/s are seen to remain relatively stable in the working section; in Figure 5 positive and negative velocities correspond to currents propagating in opposition to and following with the waves. In principle, for the profiles acquired along the flume, Figure 5 (a) and (b), higher and lower mean velocities are consistently reported at approximately 5cm below the water surface and about 2cm above the glass floor. More importantly, the relatively good overlap between the velocity profiles indicates that downstream changes in the current are not significant and thus quasi-steady flow conditions are confirmed. A similarly good agreement is reported for the profiles taken across the flume at the focus point for the waves, Figures 5 (c) and (d). Nevertheless, at the AMP (4m/1m from the wavemaker/profiler) and for following currents only, the mean velocities are seen to reduce between about 0.35m and 0.45m from the bed before increasing again to reach maximum at the surface, while the velocity profile for the next measuring station (6.9m from the wavemaker) is seen to acquire a shape similar to the profile observed at FP.

Previously, experimental (ADV) flow measurements and CFD simulations for an 'up-welling' flume showed a reduction in the mean flow velocity 15cm above the bed, and maximum turbulence intensity of (approx.) 12% for profiles acquired approximately 0.8m from the inlet, (Robinson et al., 2015). For the flow measurements presented in this paper, maximum turbulence intensity reduces from about 15% at AMP to about 7% at FP for the fastest following current, and from about 13% (AMP) to 5% (FP) for the fastest adverse current; flow measurements conducted at mid depth (e.g. for Figure 5, -0.2m < Distance from the bed < -0.3m) gave the highest turbulence intensity observations at all measuring stations. Reduced turbulence levels for adverse currents are attributed to a greater distance between the flow entry location and the impellers, see also Figure 3.

Application example

Examples of the proposed methodology for the generation of focused waves on still water and over the fastest following and adverse currents with U_s = 0.4m/s are presented first. A wideband Gaussian spectrum with peak frequency Fr_p = 0.6Hz (GW06) is selected as the target spectrum, and the AMP and the FP are set at 4m and 8.7m from the wavemaker, respectively. In preliminary tests (not presented here) 8.7m was found to be the furthest from the wavemaker location for which the focused wave was not contaminated by spurious long wave reflections. Therefore, in the figure showing the surface elevation time histories, the focus location is set at 0m with the wavemaker at -8.7m. Waves propagate in the negative direction towards the focus time at 0sec. 7 wave probes were used to measure the wave surface elevation with a sampling frequency of 100Hz, Figure 3.

For a fixed water depth of 0.5m the wave components of the target spectrum propagate in the shallow to intermediate depth regime; k_pd = 0.968, where k_p is the peak frequency wave number. The wavemaker used operates with a discrete input spectrum with ΔFr = 1/128Hz, for a selected return period of 128sec. For clarity, the wave groups are categorised based on the linear sum of the target amplitude components at focus (A). As such, wave groups with A = 0.025m are referred to as linear, and groups with A = 0.05m and A = 0.07m as weakly and strongly nonlinear, respectively. Wave groups with constant phase shifts of $\Delta\Phi = \pi n/2$, with n = 0,1,2,3, are created and the 1st order / linearised part of the spectrum is isolated using the decomposition technique described in Section 2.1.

Focused waves with A up to 0.07m are produced with an excellent agreement between the target and the measured (linearised) amplitude and phase spectrum at the AMP and the FP as shown by the solid lines in Figure 6 (a), (b) and (c). However, during the experiments it was observed that the generation of wave groups was not possible for waves steeper than H/L > 0.04 at the AMP; H/L is calculated for the largest wave in the group using a zero down-crossing method to define the wave period and the dispersion equation to calculate L. Attempts to increase further the wave steepness resulted in waves breaking before the AMP, either in the vicinity of the wavemaker or at the flow conditioner, Figure 7.

In tests conducted prior to the installation of the flow-shaping apparatus limiting non-breaking conditions were observed for a focused wave with a wide Gaussian spectrum (GW06) and A = 0.09m. Measured at 4m from the wavemaker (AMP), the steepest wave in this wave group had H/L = 0.05.

For the tests with adverse currents, focused waves with A = 0.025, 0.05, 0.07 and 0.09m were successfully generated, Figure 6 (a). In contrast, for experiments with following currents and still water, the highest focused waves generated had A = 0.05m and A = 0.07m, respectively. In fact, even for wave groups with moderate amplitude, iterations did not fully converge for frequencies higher than about 0.93Hz, dotted line in Figure 6 (b), and an undershoot was observed for the phases of these components at focus, Figure 6 (c). Nevertheless, the latter was not seen to have a noticeable effect on the behavior of the main event at focus most probably due to the small amplitude of these wave components. Examples of surface elevation records at AMP for A = 0.05m are given in Figure 6 (d). Attempts to produce focused waves with larger amplitudes either in experiments with following current or with still water resulted in waves breaking near the wavemaker.

Results

The applicability of the proposed methodology was investigated for a range of target spectra and for cases where wave frequency blockage due to adverse currents is predicted (Mei, 1983). Experimental conditions summarised in Table 1 include spectra with Fr_p = 0.6Hz and Fr_p = 0.9Hz, following and adverse currents with U_s = 0.2m/s and U_s = 0.4m/s. Shapes of target spectra can be seen in Figures 8 and 9, and bandwidths for the narrow (GN) and wide (GW) band Gaussian spectra were selected to represent the bandwidth of the JONSWAP (JS) and PM spectra, respectively.

Small wave amplitudes usually required 2 iterations, while very good focusing was achieved for the largest waves on all flow conditions within 2 or 3 further iterations. Figure 8 illustrates a range of examples for waves generated on following (dotted lines) and adverse (dashed lines) currents. For clarity, cases with waves on still water are omitted from the figure. In particular, Figure 8 (a) shows the fully nonlinear surface elevation at FP for waves generated on following and adverse current with U_s = 0.2m/s, using a PM target spectrum with Fr_p = 0.6Hz. For both tests, the linearized amplitude spectra match the target well, and a good quality focus is achieved. Encouraging results are also presented for waves with a narrowband Gaussian spectrum (GN) and Fr_p = 0.6Hz on currents with U_s = 0.4m/s (Figure 8 (b)) for waves with a wideband Gaussian spectrum (GW) and Fr_p = 0.9Hz on currents with U_s = 0.2m/s (Figure 8 (c)) and for waves with a JONSWAP spectrum (JS) and F_rp =0.6Hz on currents with U_s = 0.2m/s (Figure 8 (d)).

For waves approaching breaking, increasing the amplitude of the input signal in smaller increments allowed the effective detection of wave breaking. The latter is better illustrated in Figure 9. For a JS09 target spectrum and still water, up to limiting non-breaking waves (A = 0.07m) were successfully produced; however, breaking was observed for the largest waves on following and adverse currents with U_s = 0.2m/s (Figure 9 (a)). Increasing the input signal for following currents and moderate wave steepness (A = 0.05m) by 40% (A = 0.07m) led to waves breaking before the AMP, resulting in a diverged amplitude spectrum (Figure 9 (c)). It is, however, noteworthy that despite this and the appearance of irregularities on the following wave train, the focus quality of the main crest/event is not significantly affected (Figure 9 (b)). Results for Us = 0.4m/s demonstrated a similar trend but for small and moderate wave amplitudes. Considering the slower adverse current, attempts to increase the target amplitude from A = 0.05m to 0.06m led to amplitude (Figure 9 (d)) and phase (Figure 9 (e)) convergence but breaking was observed between the FP and AMP.

Finally, for experiments looking at wave groups with Fr_p =0.9Hz on the strongest (U_s = 0.4m/s) adverse currents, wave blocking of high frequency components at the AMP is reported. Blocking of the higher frequency parts of the wave spectrum is a well-documented aspect of wave-structure interaction and for waves on a depth uniform current it occurs at points where the wave group velocity is equal to that of the current, e.g. (Chawla and Kirby, 2002). Figure 10 (a) and (b) show the amplitude spectra of the linearized part at the AMP for wave groups produced with a wideband Gaussian and a JONSWAP target spectrum, while the phase spectrum at focus is presented in Figure 10 (c) and (d). For both cases, blocking is seen to occur for wave components with frequencies greater than about 1Hz.

Conclusions

A methodology to focus steep wave groups on currents has been developed and applied in a specifically designed experimental apparatus for creating sheared currents in a wave-current flume. For the ‘up-welling’ type flume available to this study the use of the suggested flow conditioning/profiling arrangement resulted in relatively stable, collinear sheared velocity profiles for currents of different velocities flowing following or opposing the direction of wave propagation, and with turbulence intensity levels acceptable for studies representative of real sea conditions. The conditions reproduced here resemble those reported for the Pentland Firth, UK (Chatzidou and Karunarathna, 2014).

Focused wave groups with the same initial amplitude spectrum near the wavemaker are reproduced for a range of flow conditions, including still water, following and adverse sheared currents with different magnitudes. Target spectra with and without equilibrium tails are used as targets, and phase focusing at the same location is illustrated for all cases including those with strongly nonlinear waves. The well-known problem of spatial and temporal down-shifting of the focus point is thus overcome. Clearly, the need to generate waves with 4 phase shifts for each iteration is a disadvantage, somewhat balanced, however, by the ability to use the corrected input signal to generate the same wave on the same flow conditions in future experimental expeditions involving, for example, structures installed at the focus location.

To the best of the authors' knowledge this is the first time that such detailed control of the generation of focusing wave groups on sheared currents has been achieved. Here this work is considered an improvement on existing methodologies for conducting experimental studies into wave-current and wave-current-structure interaction.

Acknowledgments

The authors are thankful to EPSRC for supporting this project within the Supergen Marine Technology Challenge (Grant EP/J010316/1)

References

Banner, M. L., and Song, J. B. (2002) On determining the onset and strength of breaking for deep water waves. Part II: Influence of wind forcing and surface shear. Journal of Physical Oceanography, 32, 2559.

Baldock, T.E., Swan, C., and Taylor, P.H. (1996) A laboratory study of nonlinear surface waves on water. Phil. Trans. R. Soc. Lond. A., 354 (1707), 649-676.

Borthwick, A., Hunt, A., Feng, T., Taylor, P., and Stansby, P. (2006). Flow kinematics of focused wave groups on a plane beach in the U.K. coastal research facility. Coastal Engineering, 53, 1033–1044.

Bretherton, F. P., and Garrett, G. J. R. (1968) Wave trains in inhomogeneous moving media. Proc. Of the Royal Society London, A 1968 302 529-554.

Buldakov D., Stagonas, D., and Simons R. (2017) Extreme Wave Groups in a Wave Flume: Controlled Generation and Breaking Onset. Coastal Engineering. Vol. 128, October 2017, Pages 75–83.

Chanson, H., Trevethan, M., and Koch, C., (2007) Discussion of turbulence measurements with acoustic Doppler velocimeters by Carlos M. García, Mariano I. Cantero, Yarko Niño, and Marcelo H. García. ASCE 133, 1283–1286.

Chaplin, J.R. (1996) On frequency-focusing unidirectional waves. International Journal of Offshore and Polar Engineering, 6(2), 131-137.

Chatzirodou, A., and Karunarathna, H. (2014) Numerical modelling of sea bed morphodynamics associated with tidal energy extraction, 3rd Oxford Tidal Energy Workshop, Oxford, UK.

Chawla, A., and Kirby, J.T. (2002) Monochromatic and random wave breaking at blocking points. Journal of Geophysical Research: Oceans. 107, 2156-2202.

Christou, M., and Ewans, K. (2014) Field measurements of rogue water waves. Journal of Physical Oceanography, 44(9), 2317–2335.

Dingemans, M. W (1997) Water Wave Propagation Over Uneven Bottoms (In 2 Parts). Advanced Series on Ocean Engineering, World Scientific, Singapore.

Fernandez, H., Sriram, V., Schimmels, S., and Oumeraci, H.(2014). Extreme wave generation using self-correcting method - revisited. Coastal Engineering, 93, 15–31.

Fitzgerald, C., Taylor, P., Eatock Taylor, R., Grice, J., and Zang,J. (2014). Phase manipulation and the harmonic components of ringing forces on a surface-piercing column. Proc. of the Royal Society A: Mathematicsal, Physical and Engineering Sciences, 470 20130847.

Giles, J., Myers, L., Bahaj, A. B., and Shelmerdine, B. (2011) The Downstream Wake Response of Marine Current Energy Converters Operating in Shallow Tidal Flows. Proceedings of the World Renewable Energy Congress, Linköping University, 2270-2277.

Hann, M., Greaves D., and Raby, A. (2014) A new set of focused wave linear combinations to extract nonlinear wave harmonics. Proceedings of the 29th International Workshop on Water Waves and Floating Bodies, Osaka, Japan.

Kemp, P. H., and Simons, R. R. (1982) The interaction of waves and a turbulent current – waves propagating with the current. Journal of Fluid Mechanics, 116, 227 - 250.

Kemp, P. H., and Simons, R. R. (1983) The interaction of waves and a turbulent current – waves propagating against the current. Journal of Fluid Mechanics, 130, 73 - 89.

Lindgren, G. (1970) Some properties of a normal process near a local maximum. Ann. Math. Stat., 41(6), 1870–1883.

Mei, C. C., (1983) The Applied Dynamics of Ocean Surface Waves. *John Wiley & Sons*, 740 pp.

Orszaghova, J., Taylor, P. H., Borthwick, A. G., and Raby, A. C. (2014) Importance of second-order wave generation for focused wave group run-up and overtopping. Coastal Engineering, 94, 63–79.

Peregrine, D. H. (1976) Interaction of water waves and currents. Adv. Appl. Mech., 16, 9–117.

Rapp, R.J., and Melville W.K. (1990).Laboratory measurements of deep water breaking waves. Philos. Trans. R. Soc. London. Ser A 331, 735-800.

Robinson, A. Ingram, D., Bryden, I., and Bruce, T. (2015) The effect of inlet design on the flow within a combined waves and current flumes, test tank and basins. Coastal Engineering, 95, 117–129.

Rusello, P.J., Lohrmann, A., Siegel, E., and Maddux, T., (2006) Improvements in Acoustic Doppler Velocimetery. Proceedings of the 7th International Conference on Hydroscience and Engineering, Philadelphia, USA.

Schmittner, C., Kosleck, S., and Henning J. (2009) A phase-amplitude iteration scheme for the optimization of deterministic wave sequences. Proceedings of the 28th International Conference on Offshore Mechanics and Artic Engineering, 1-8.

Shemer, L., Goulitski K., and Kit E. (2007) Evolution of wide-spectrum unidirectional wave groups in a tank: an experimental and numerical study. European Journal of Mechanics B/Fluids, 26, 193-219.

Stagonas, D., Buldakov, E., Simons, R.R. (2014) Focusing unidirectional wave groups on finite water depth with and without currents. Coastal Engineering Proceedings, 34, p. waves.31.

Swan, C., Cummins I. P., and James R. L. (2001) An experimental study of two-dimensional surface water waves propagating on depth-varying currents. Part1: Regular waves. Journal of Fluid Mechanics, 428, 273–304.

Taylor, P., and Williams, B. (2002). Wave statistics for intermediate depth water - NewWaves and symmetry. Proceedings of the International Conference on Offshore Mechanics and Arctic Engineering, 2, 629–634.

Tromans, P. S., Anatruk, A., and Hagemeijer, P. (1991). New model for the kinematics of large ocean waves application as a design wave. Proceedings of the First International Offshore and Polar Engineering Conference, 64–71.

Yao, A. and Wu, C. H. (2005) Incipient breaking of unsteady waves on sheared currents. Physics of Fluids, 17, 082104.

Tables

Table 1: Summary of experimental conditions for waves and currents.

Wave conditions			Flow conditions	
Spectrum	Peak frequency [Hz]	Amplitude [m]	Current	Surface Velocity [m/s]
Wide Gaussian (GW)	0.6Hz	0.025, 0.05, 0.07	Still water, Adverse, Following	0, ±0.2, ±0.4
	0.9Hz	0.025, 0.05, 0.07	Still water, Adverse, Following	0, ±0.2, ±0.4
Narrow Gaussian (GN)	0.6Hz	0.025, 0.05, 0.07	Still water, Adverse, Following	0, ±0.2, ±0.4
	0.9Hz	0.025, 0.05, 0.07	Still water, Adverse, Following	0, ±0.2, ±0.4
JONSWAP (JS)	0.6Hz	0.025, 0.05, 0.07	Still water, Adverse, Following	0, ±0.2, ±0.4
	0.9Hz	0.025, 0.05, 0.07	Still water, Adverse, Following	0, ±0.2, ±0.4
Pierson-Moskowitz (PM)	0.6Hz	0.025, 0.05, 0.07	Still water, Adverse, Following	0, ±0.2, ±0.4
	0.9Hz	0.025, 0.05, 0.07	Still water, Adverse, Following	0, ±0.2, ±0.4

Figure

Click here to download Figure Figure 1_300.tiff

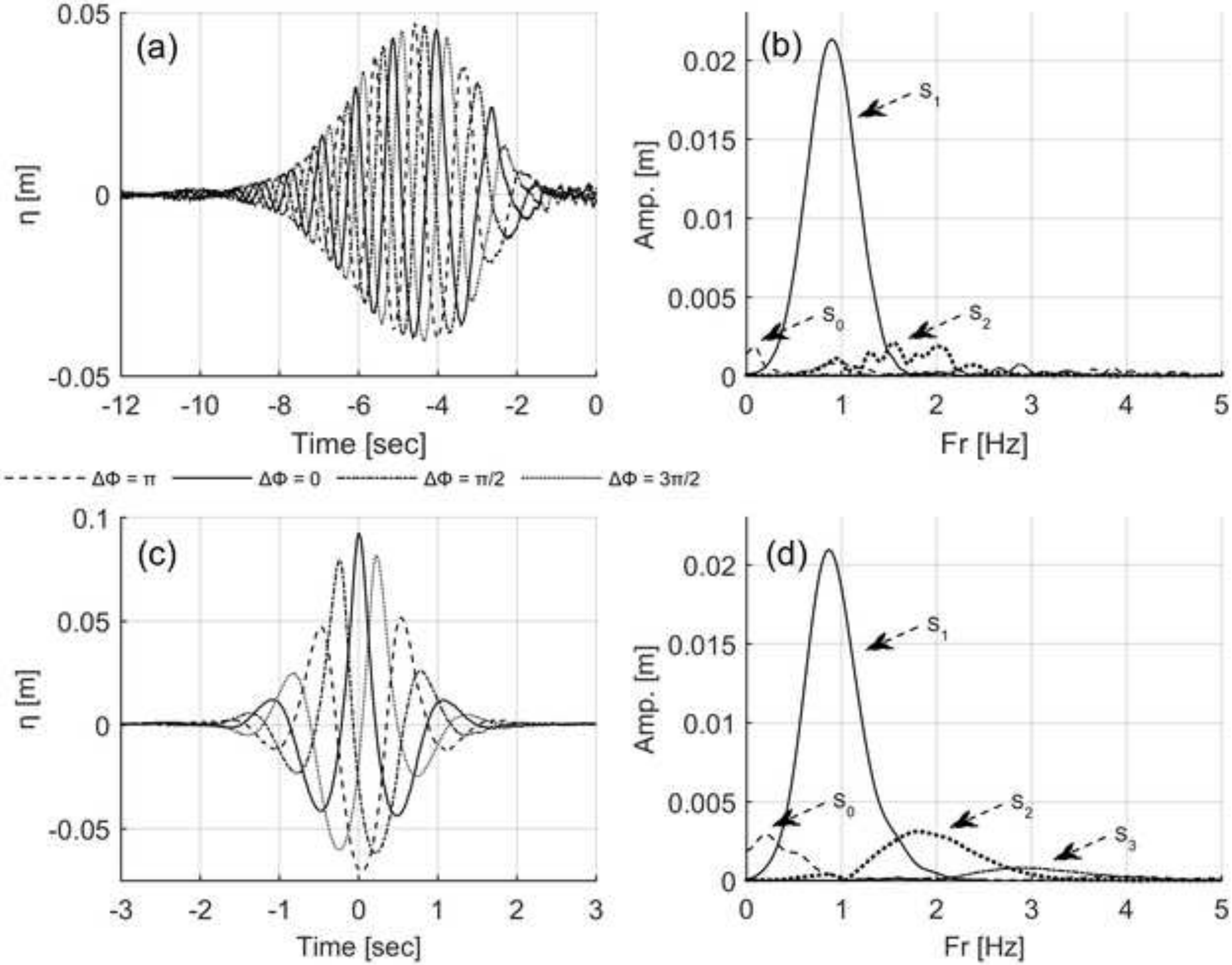

Figure

Click here to download Figure Figure 2_300.tiff

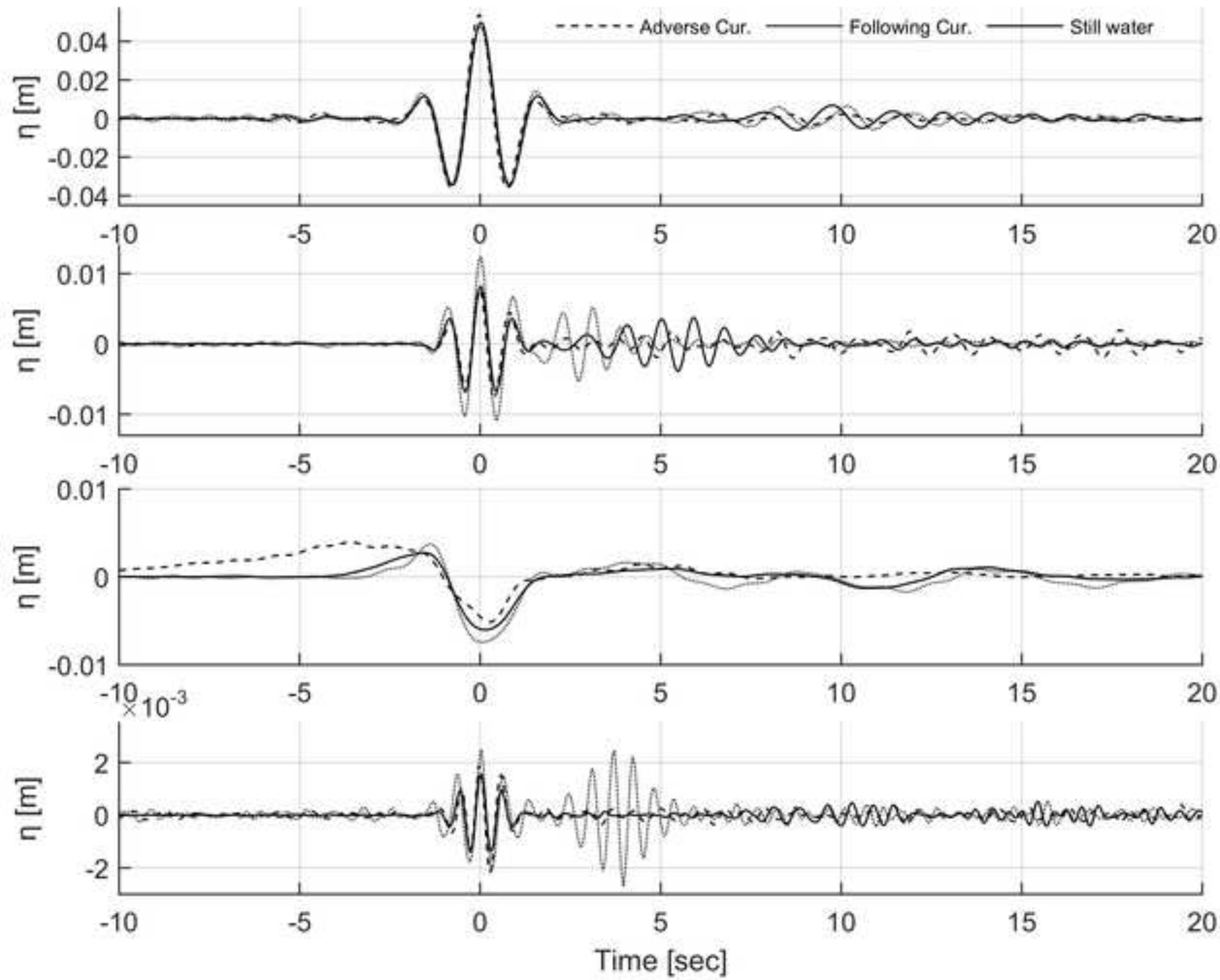

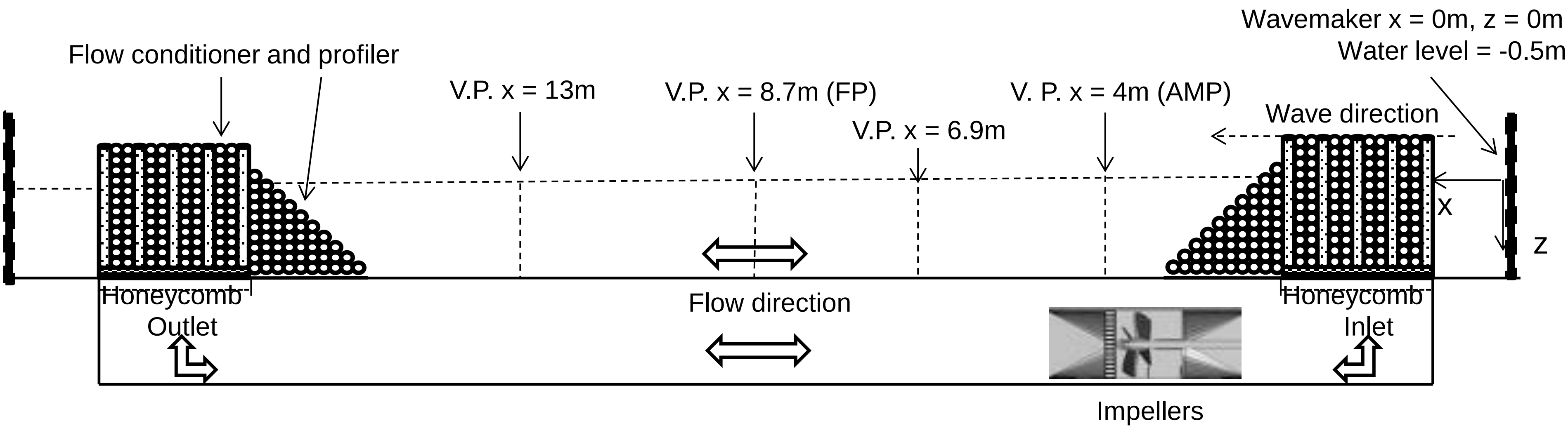
Wavemaker x = 0m, z = 0m
Water level = -0.5m
Flow conditioner and profiler
V.P. x = 13m
V.P. x = 8.7m (FP)
V. P. x = 4m (AMP)
V.P. x = 6.9m
Wave direction
X
Z
Honeycomb
Outlet
Flow direction
Honeycomb
Inlet
Impellers

Figure

Click here to download Figure Figure 5_300.tiff

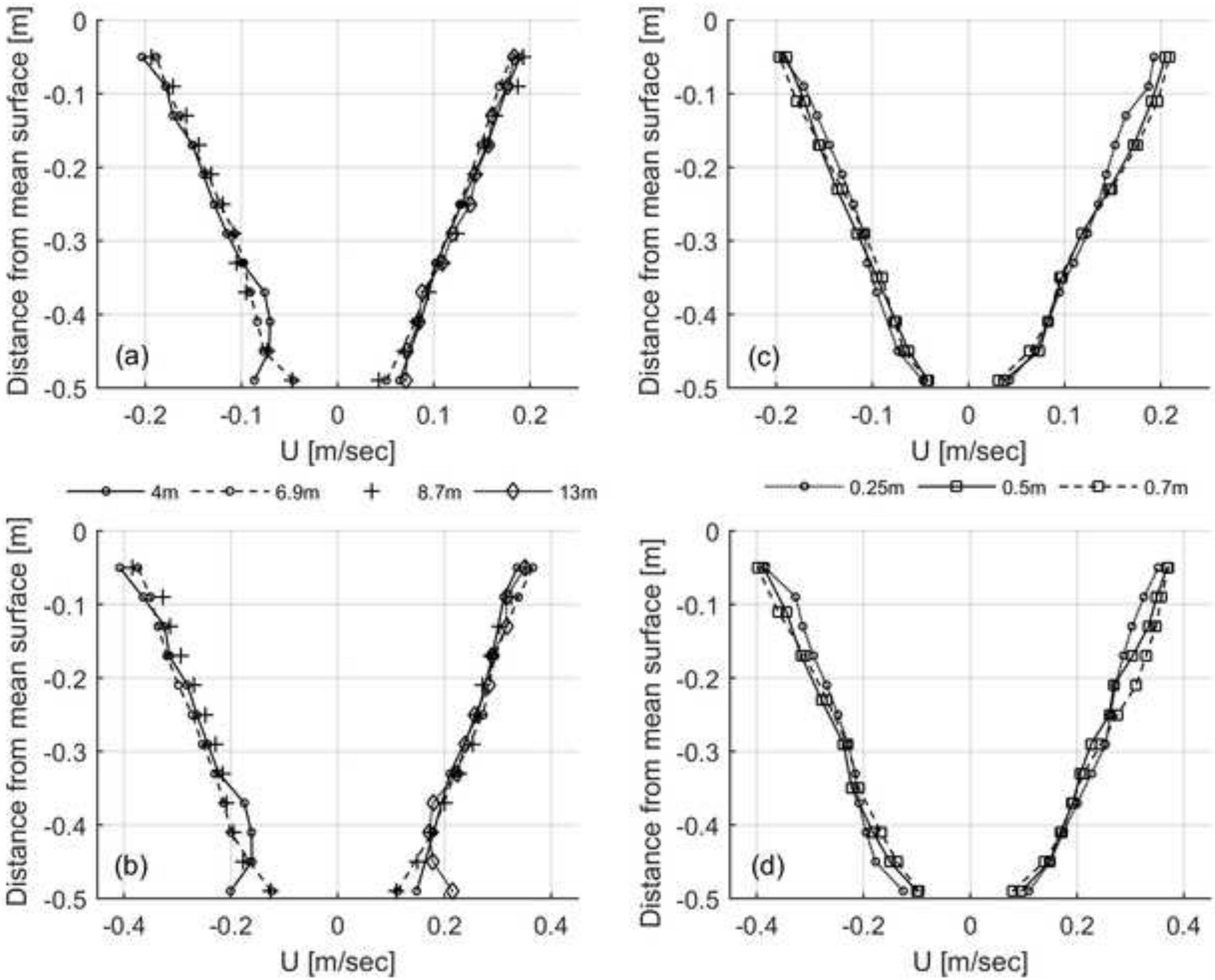

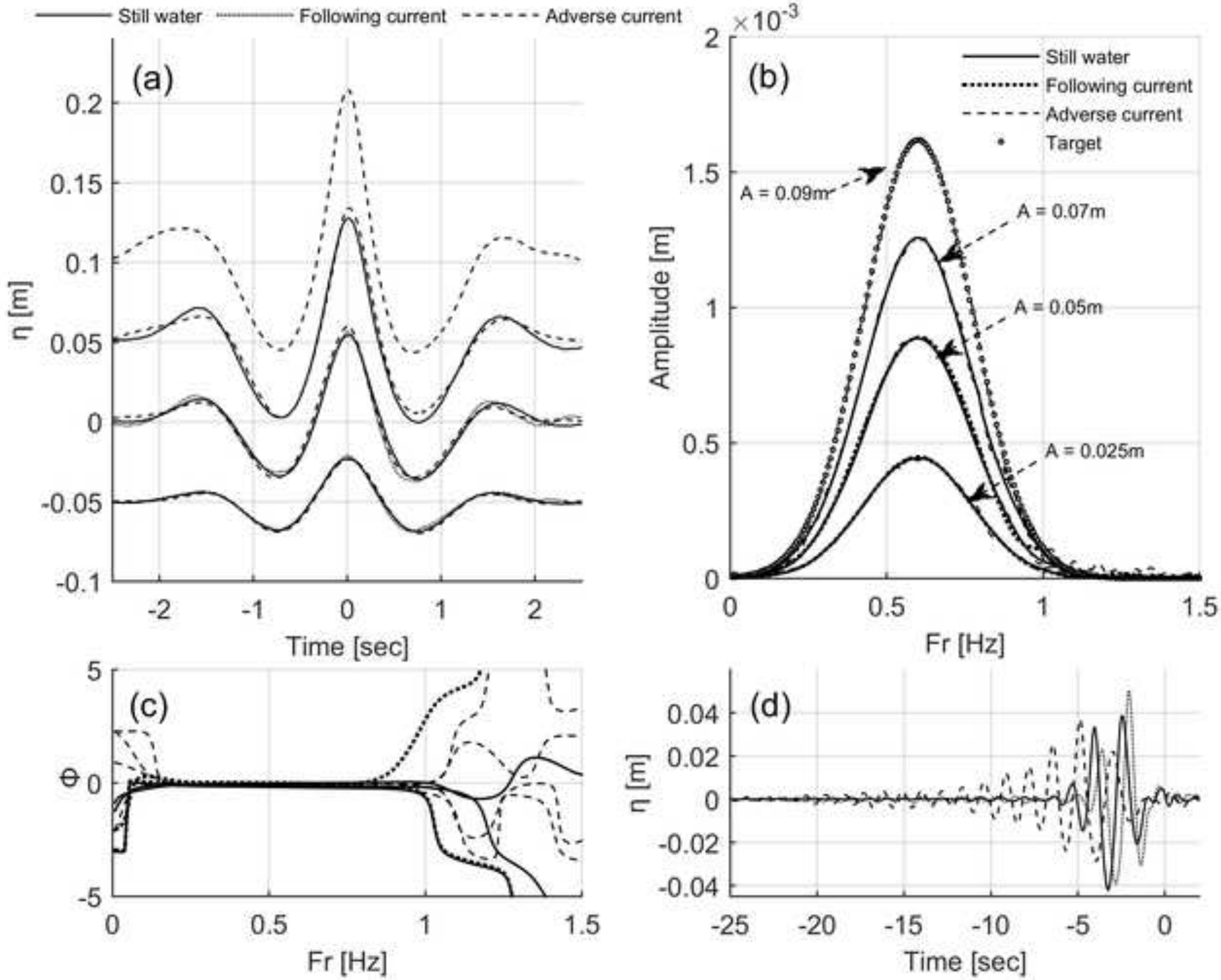
Still water
Following current
Adverse current
(a)
η [m]
Time [sec]
(b)
Amplitude [m]
×10^-3
Target
A = 0.09m
A = 0.07m
A = 0.05m
A = 0.025m
Fr [Hz]
(c)
Φ
Fr [Hz]
(d)
η [m]
Time [sec]

Figure

Click here to download Figure Figure 8_300.tiff

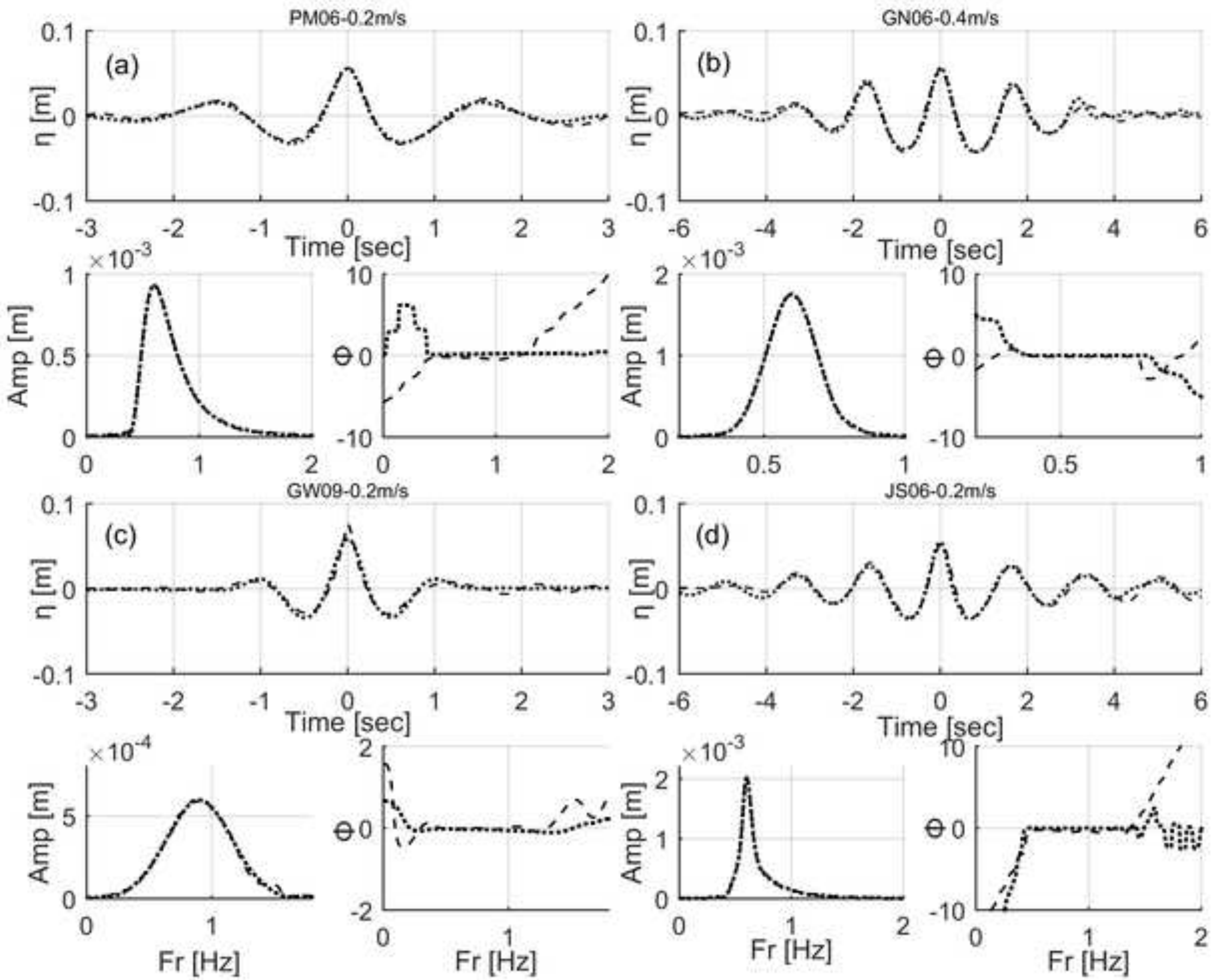

Figure

Click here to download Figure Figure 9_300.tiff

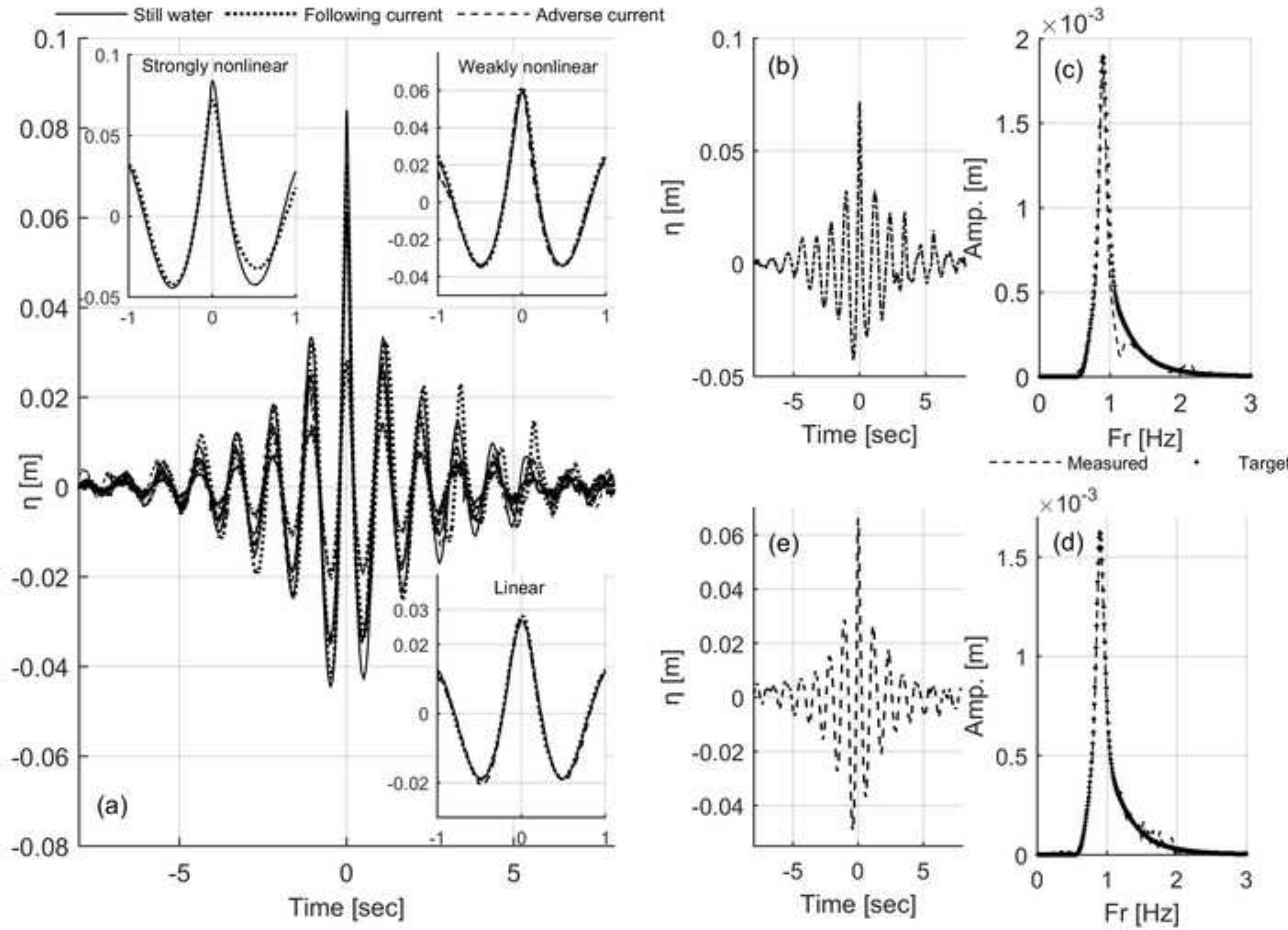

Figure

Click here to download Figure Figure 10_300.tiff

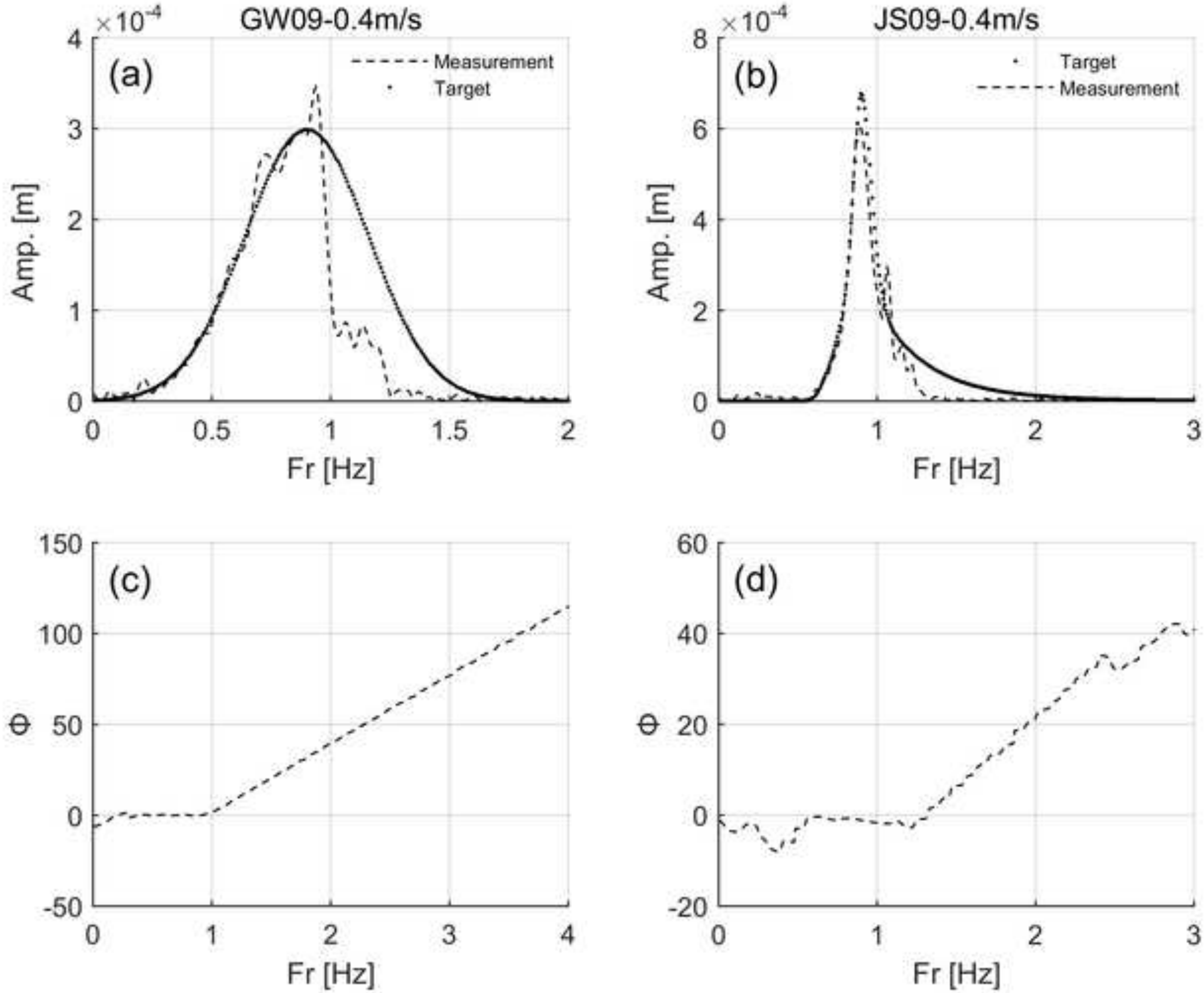

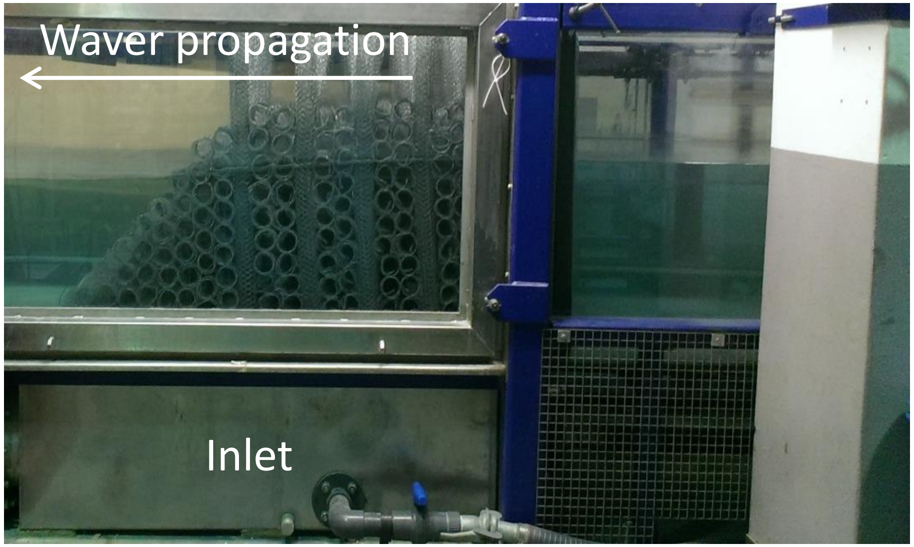
Waver propagation
Inlet

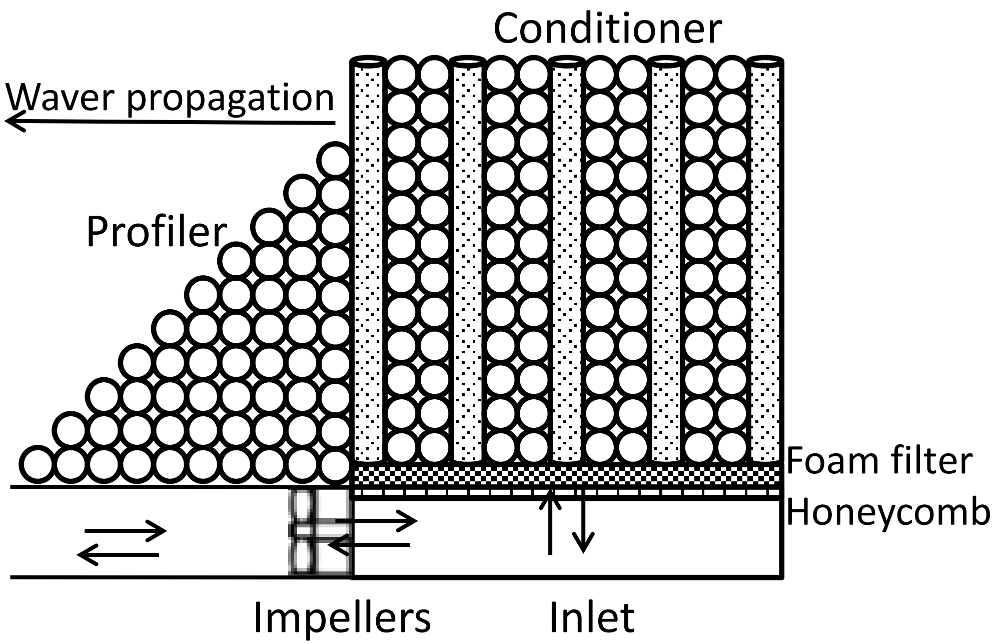
Conditioner
Waver propagation
Profiler
Foam filter
Honeycomb
Impellers
Inlet

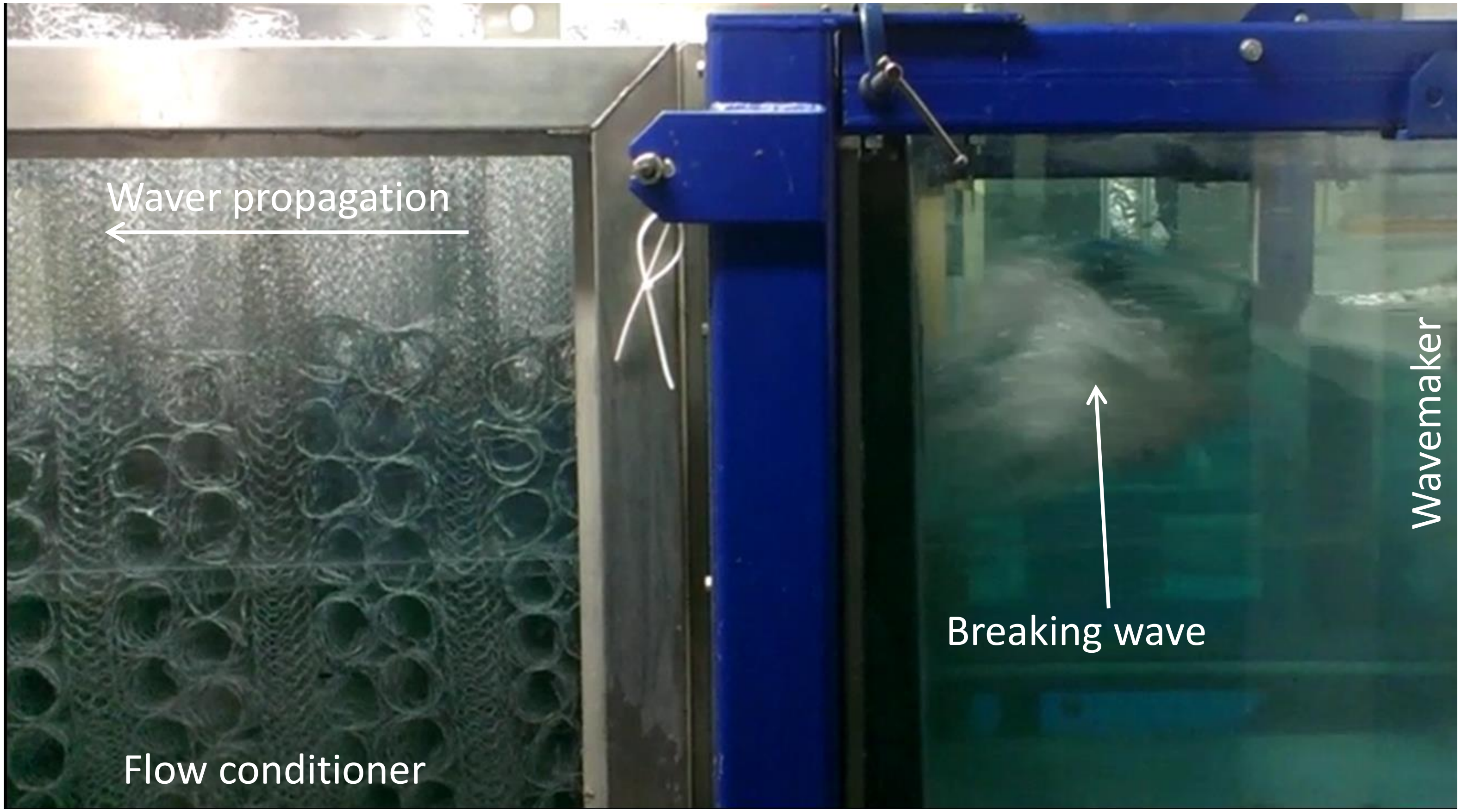
Waver propagation
Wavemaker
Breaking wave
Flow conditioner

Captions

Figure 1: (a), surface elevation measurements at AMP for wave groups generated on still water with $\Delta\Phi = 0, \pi, \pi/2, 3\pi/2$. (b) and (d), decomposed amplitude spectra at AMP and FP; for $S_{0,1,2,3}$ see Eq.3. (c), surface elevation measurements at FP for $\Delta\Phi = 0, \pi, \pi/2, 3\pi/2$. Target spectrum: wideband Gaussian (GW), Fr_p = 0.9Hz and A = 0.07m.

Figure 2: Surface elevation time histories reconstructed at FP using Inverse Fourier Transformation. (a) linearised, (b) 2nd order sum, (c) 2nd order difference, and (d) 3rd and higher order part. Target spectrum: wideband Gaussian, Fr_p = 0.6Hz, A = 0.05m and U_s = 0.4m.

Figure 3: 2D stream-wise slice of the UCL wave-current flume. (x, z) = (0m, 0m) is set at the intersection of the wavemaker with the water level. Marked with V.P. are the locations for the mean velocity profile measurements. For all tests, wave probes were set at x = 4, 5.7, 6.9, 7.7, 8.2, 8.45 and 8.7m.

Figure 4: Photograph (on the left) and schematic (on the right) of the flow shaping arrangement.

Figure 5: (a) and (b), mean velocity profiles measured along the flume. Negative and positive velocity values correspond to cases on following and adverse currents, respectively. For (a) and (c) U_s = 0.2m/s, while for (b) and (d) U_s = 0.4m/s.

Figure 6: (a), time histories of surface elevation measured at focus. For clarity a constant amplitude shift of ±0.05m has been added. Linear (A = 0.025m), weakly (A = 0.05m) and strongly (A = 0.07m) nonlinear waves groups are plotted at -0.05, 0m and +0.05m, respectively. For adverse currents, waves with A = 0.09m were also generated and are plotted with a dashed line at 0.1m. (b), linearised amplitude spectra at the AMP. (c), linearised phase spectra at focus, and (d), fully nonlinear surface elevation measurements at the AMP for wave groups with A = 0.05m. Target spectrum: wideband Gaussian (GW), Fr_p = 0.6Hz, U_s = 0.4m/s.

Figure 7: Snap-shop of a wave breaking near the wavemaker (not shown), for GW06 and A = 0.07m on following current with U_s = 0.2m/s

Figure 8: Surface elevation measurements at focus, linearised amplitude spectra at the AMP and phase spectra at the FP are presented for different test cases. (a), target spectrum: Pierson-Moskowitz (PM), Fr_p =0.6Hz, U_s = 0.2m/s. (b), experiments with a narrowband Gaussian (GN) target spectrem,

Fr_p = 0.6Hz, U_s = 0.4m/s. (c) target spectrum: wideband Gaussian (GW), Fr_p =0.9Hz, U_s = 0.2m/s. (d) JONSWAP (JS), Fr_p = 0.6Hz, U_s = 0.2m/s. Still water measurements are omitted for clarity. For all graphs, dotted lines: waves on following current and dashed lines: waves on opposing current.

Figure 9: (a), time histories of surface elevation at focus for A = 0.025m , A = 0.05m and A = 0.07m. (b) and (c), surface elevation measurements at the FP and linearised spectrum at the AMP for A = 0.07m on following current, U_s = 0.2m/s. (d) and (e), time histories of surface elevation at focus and linearised spectrum at the AMP for A = 0.06m on adverse current, and U_s = 0.2m/s. Target spectrum JONSWAP, Fr_p = 0.9Hz.

Figure 10: Linearised amplitude ((a) and (b)) and phase ((c) and (d)) spectra at the AMP and the FP, respectively. All wave groups were generated with Fr_p =0.9Hz and A = 0.025m, on adverse current with U_s = 0.4m/s. Target spectrum: (a) and (c), wideband Gaussian and (b) and (d), JONSWAP.